Scattering Modeling of Nucleation Gels

Che-Min Chou and Po-Da Hong*

Department of Polymer Engineering, National Taiwan University of Science and Technology, Taipei 10607, Taiwan

Received April 9, 2008; Revised Manuscript Received June 20, 2008

ABSTRACT: On the basis of elastic scattering theory, we propose a methodological framework to exactly reconstruct the entire course during the structural formation of the nucleation gel. The focus of the present work is on command of the interaction relations between scattering factors and on understanding of how and to what extent these interactions obtain information on aspects of a complex event in gelation. The scattering modeling provides a much more detailed and direct examination on the quantitative structure−evolution relationship and differentiates the gelation process into−nucleation and growth, aggregation, diffusion-controlled coarsening (fast process), and Ostwald ripening (slow process)−four stages in which the kinetic evolutions are predicted by either the growth or the coarsening theory. We demonstrate that the scattering modeling can be practically implemented, can provide valuable results, and would serve as the basis for a study of temporal and spatial complexity of soft matter on a mesoscopic length scale.

1. Introduction

The majority of researches in the physical gels have focused on the "microscopic" junction structure and the "macroscopic" viscoelastic properties. Guenet[1]and te Nijenhuis[2] have provided extensive discussions on the subjects. In reality, the structure of physical gels is too involved; however, the traditional viewpoint ("equilibrium") and classification ("junction basis") frequently do not give a realistic description of how the diverse, hierarchical morphologies of physical gels are formed. The key is that the "microscopic" structure and the "macroscopic" properties are not necessarily mutually deducible. Despite the growing awareness of the micro−macro linkage, there has thus far been relatively little research into the area. Most findings on gel structural formation have been descriptive and have up to now employed "morphological criteria" to−imaginatively−reconstruct the gelation process.[3,4]

In the first attempt to explore the origin of the diverse gel morphologies, we used time-resolved small-angle light scattering (SALS) to trace the gelation process of PVDF solutions.[5−7] We proposed a new model in which the course of the gelation includes−nucleation and growth, aggregation, percolation, and coarsening−four consecutive processes, called the "nucleation gel". While the nucleation gel is a widespread phenomenon,[8−10] the situation is even less understood. Our series of works have so far presented a fairly clear picture of at least some basic issues. First, unlike the traditional viewpoint,[1−4] the definition of the "nucleation" is not on the localized junction "point" but really involves a mesoscopic length scale over; thus, the focus of the "gelation" shifts from an emphasis on the percolation phenomena[11,12] to attention to the aggregation behavior. Second, even though the large-scale heterogeneous gels are widely believed to result from spinodal decomposition ("spinodal gel"),[13−17] their formation might be of a rather different origin. Third, the nature of nucleation gel is purely nonequilibrium phenomena, and the concept itself blurs the boundary between the gel ("elastic" and three-dimensional network structure) and the jammed solid ("fragile" and nonequilibrium solid state).[18,19] Although the discussion has been restricted so far to a phenomenological level, the nucleation gel gives us new opportunities to deal in a more general manner with the physical gelation.

* Corresponding author: Fax +886-2-27376544, e-mail poda@mail.ntust.edu.tw.

Using the scattering technique to exactly reconstruct a complicated structure is one of the more intriguing subjects. A recent development is the combining different scattering techniques to study a "spacial" hierarchical structure in multiscale systems.[20−22] In contrast to these great advances, although the basic depolarized (H_v) scattering theories have been provided for several decades,[23,24] the application of the H_v scattering technique to complicated aggregation systems has only been touched upon so far. One of the thorniest problems researchers face is that extracting all structural information contained in H_v scattering patterns is often not trivial. At this point, we have obtained some remarkable progress especially on H_v scattering from birefringent sphere and its aggregation.[7] With this finding we now have all the ingredients to allow for a reliable analysis of the complicated nucleation gel. In this paper, we try to extend the H_v scattering technique to the more realistic case of both "spacial" and "temporal" mesostructural evolution and to demonstrate the practicability of the scattering modeling through the nucleation gel. Results of the present study represent the most complete modeling process to date in obtaining information on aspects of a complex event in gelation and provide new insights into both the scattering methodology and the science of gelation.

2. Background

2.1. Scattering Factors. We have proposed three phenomenological functions to describe the nucleation gel. In our model, the H_v scattering function $I_{H_v}(q,\varphi)$ can be written as[6]

$$I_{H_v}(q,\varphi) \sim P_{H_v}(q,\varphi)\, S(q)\, f(q) \tag{1}$$

where $P_{H_v}(q,\varphi)$ is the form factor, which describes the scattering of a spherical particle along and depends on the azimuthal angle φ, $S(q)$ is the structure factor, which describes the spatial arrangement of the particles within a cluster, and $f(q)$ is the interference function of two interpenetrated spheres, which describes how the local structure of the nucleation gel evolves in late-stage coarsening.

The form factor is given by[24]

$$P_{H_v}(q,\varphi) = C|S_2 - S_1|^2 \sin^2 2\varphi \tag{2}$$

where C is a constant depending on the apparatus setup. The expressions for S_1 and S_2 in the Rayleigh−Gans−Debye light scattering approximation are[24]

10.1021/ma800788j CCC: $40.75 © 2008 American Chemical Society
Published on Web 08/14/2008

$$S_1 = \frac{2ik^3a^3}{3x^3}\{3(\mu-1)(\sin x - x\cos x) + \Delta\mu[x\cos x - 4\sin x + 3Si(x)]\} \quad (3)$$

and

$$S_2 = \frac{2ik^3a^3}{3x^3}\{3(\mu-1)(\sin x - x\cos x)\cos\theta - \Delta\mu[1+\cos^2(\theta/2)][x\cos x - 4\sin x\, Si(x)]\} \quad (4)$$

where a is the spherical radius, x is defined by $x = qa$, μ is the relative mean refractive index of the sphere, $\Delta\mu$ is the birefringence index, and $Si(x)$ is the sin integral defined by

$$Si(x) = \int_0^x \frac{\sin u}{u}\,du \quad (5)$$

If the birefringent sphere is surrounded by an isotropic medium of refractive index m_1, then μ is defined by $\mu = (m_r + 2m_t)/3m_1$ and the $\Delta\mu$ is defined by $\Delta\mu = (m_r - m_t)/m_1$, where m_r and m_t are the radial and tangential refractive indices of the sphere, respectively. In reality, a more or less broad particle size distribution is established; thus[25]

$$I = \int_0^\infty n(a)\, I(a)\, da \quad (6)$$

where $n(a)$ is a size distribution function of the sphere. As the simplest example, we assumed a Gaussian distribution function

$$n(a) = \exp\left[-\frac{1}{2}\left(\frac{a-a_0}{\beta}\right)^2\right] \quad (7)$$

where a_0 is average radius of the spheres in the distribution and β is the half-width of the distribution.

The structure factor is given by[26]

$$S(q) = 1 + \frac{D_f\Gamma(D_f-1)}{(qa_0)^{D_f}(1+1/q^2\xi^2)^{(D_f-1)/2}}\sin[(D_f-1)\tan^{-1}(q\xi)] \quad (8)$$

where ξ is the characteristic correlation length of the aggregate and is related to the radius of gyration by $\xi^2 = 2R_g^2/[D_f(D_f-1)]$, where $R_g \sim a_0N^{1/D_f}$, D_f is the fractal dimension, N is the number of primary particles or monomers in the aggregate, and $\Gamma(x)$ is the gamma function.

The interference function can be written as[6,27]

$$f(q) = \frac{\frac{1}{2} + J_0(2ka_rF\sin\theta)}{a_r^2(2\pi - 3\arccos F + 2F\sqrt{1-F^2})} \quad (9)$$

where J_0 is the zero-order Bessel function, a_r is the time-dependent coarsening size, and F is the overlapping parameter defined by $F = a_0/a_r$. For two spheres in hard-sphere contact, $F = 1$. If the coarsening of two contact spheres, $F < 1$.

2.2. Scattering Modeling. The purpose of the scattering modeling approach is to capture the essence of a phenomenon with the simplest possible way. It is helpful to describe two basic principles before moving on to the main task. The first principle is the multiplication. When the interacting particles aggregate into a cluster, the density−density correlation function of the aggregate can be expressed as the convolution of the single particle correlation function and the pair correlation function.[28,29] From the convolution theorem, the Fourier transform of the convolution of two functions in real space equals the pointwise multiplication of the transform of each function in Fourier space;[28] thus, the scattering function of the aggregate can be written as eq 1. The second principle is the linear superposition. If there is no correlation between the scattering clusters, the scattered intensity can be regarded as the sum of the intensities scattered by individual clusters. Hence, a simple model is expressed as follows

$$I_{H_v}(q,\varphi) \sim b'\,S(q)P^{d}_{H_v}(q,\varphi)\phi_c + c'\,F(q,\varphi)(1-\phi_c) \quad (10)$$

where $P^{d}_{H_v}(q,\varphi) = P_{H_v}(q,\varphi)f(q)$ is the scattering factor of the sphere doublet, $b' = P_{H_v,q\to\infty}/P^{d}_{H_v,q\to\infty}$, and $c' = P_{H_v,q\to\infty}/F_{q\to\infty}$ are the baseline coefficients, ϕ_c is the volume fraction of the clusters, and the transition factor $F(q,\varphi)$ is written as

$$F(q,\varphi) = P^{d}_{H_v}(q,\varphi)\phi_d + P_{H_v}(q,\varphi)(1-\phi_d) \quad (11)$$

where ϕ_d is the volume fraction of the sphere doublet. Equations 10 and 11 can easily be studied numerically once the key physical features of structure are specified. If $\phi_d = \phi_c = 0$, we recover the original expression for the birefringent sphere $I_{H_v}(q,\varphi) \sim P_{H_v}(q,\varphi)$. If $\phi_d = \phi_c = 1$, the model reduces to eq 1 and characterizes the late-stage evolution of nucleation gel. In the special case where $\phi_d \sim 1$ and $\phi_c \sim 0$, the model provides a way to examine the early stage aggregation of the birefringent spheres.

2.3. Extraction of Structural Parameters from Scattering Data. Generally, the peak position q_m defines a characteristic length by $\xi = 2\pi/q_m$.[28] However, this common rule does not direct apply to the case of the H_v scattering. The reason has two aspects. First, in addition to a_0, q_m and even with $P_{H_v}(q,\varphi)$ also depend on $\Delta\mu$;[7,30] indeed, the common criterion $qa = 4.1$ for H_v scattering is validity at $|(\mu-1)/\Delta\mu| < 0.4$.[31] Second, as discussed in our previous papers,[6,7] q_m does not inevitably characterize ξ in H_v scattering. Thus, we must use the model to fit experimental data. The model, however, consists of 10 parameters (i.e., single particle: a_0, μ, $\Delta\mu$, m_1, and β; fractal cluster: D_f, N, and ϕ_c; late-stage evolution: a_r and ϕ_d). How to better determine their behavior and to correctly understand the interaction between them is a problem.

The determination of a_0 and $\Delta\mu$ is most difficult in fitting procedure due to the fact that $\Delta\mu$, μ, and m_1 are closely linked together. Because the concentration of the solute decreases as the nuclei grows, the value of m_1 is time dependent; thus, we should reduce its contribution to μ and $\Delta\mu$. If we limit the variation of μm_1 and m_1 within the range of 1.42 (refractive index of polymer) to 1.434 (refractive index of solvent), a_0 and $\Delta\mu$ could be appropriately determined from the relationship of the scaled form factor $\tilde{P}_{H_v}(x)$ and the kinetic behavior $q_m \sim t^{-0.9}$.[6,7] On the other hand, we have demonstrated that the H_v scattering only highlights the feature of local-structure evolution;[7] thus, the long-rang fractal behavior, such as N and ϕ_c, was determined according to numerical considerations. The value of N was fixed to 50, and the behavior of ϕ_c was described by a simple power law. The temporal behavior of D_f was determined by fitting the power-law decay of the experimental $I_{V_v}(q)$ in the small q region.[6] Finally, a_r and ϕ_d were left to be floating in the fitting.

3. Experimental Section

3.1. Materials. The crystalline polymer used in this study was poly(vinylidene fluoride) (PVDF) powder ($M_w = 2.75 \times 10^5$ and $M_w/M_n = 2.75$, Aldrich Chemical Co.). The solvent was a mixture of tetra(ethylene glycol) dimethyl ether (TG) and $LiCF_3SO_3$ salt. The salt was added to give an O:Li ratio (oxygen atoms in TG: lithium atoms in the salt) of 12:1. The polymer gel electrolytes were prepared by quenching homogeneous PVDF solution from 433 K to the gelation temperature 293 K.

3.2. Time-Resolved SALS Apparatus. The optical arrangement of the time-resolved SALS apparatus has been described previously.[5] A 5 mW polarized He−Ne laser was used as the incident source, and the polarization direction of the beam was adjusted by a half-wave plate. The beam was then spatially filtered, expanded,

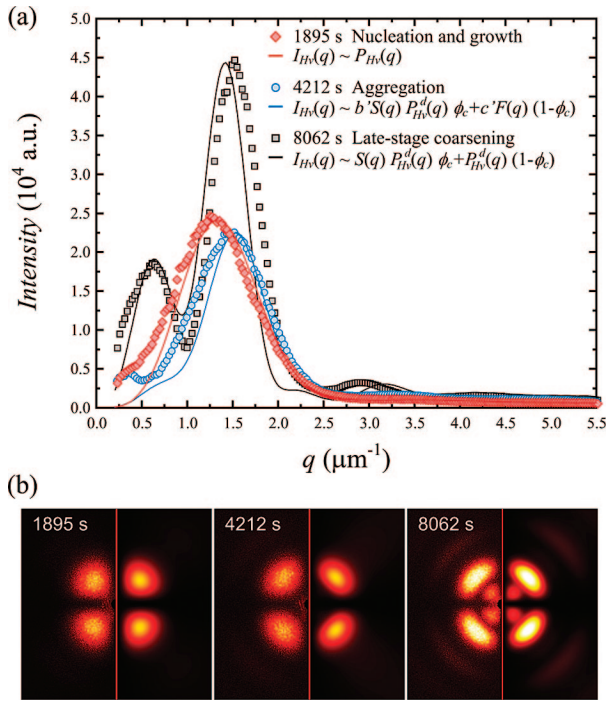

Figure 1. (a) Behavior of the H_v scattering profiles ($\varphi = 45°$) in the three stages of gelation for PVDF/TG-$LiCF_3SO_3$ solution ($\phi = 0.04$) at 293 K. The solid lines show the best-fitted theoretical scattering curves by our nucleation gel model. (b) A comparison of the experimental (left half of patterns) and the best-fitted theoretical (right half of patterns) H_v scattering patterns in the three evolution stages. The fitting parameters for nucleation and growth stage: $a_0 = 3.033$, $\mu = 0.99343$, $\Delta\mu = 1.0059 \times 10^{-4}$, $m_1 = 1.4295$, and $\beta = 0.469$; for aggregation stage: $a_0 = 3.051$, $\mu = 0.99095$, $\Delta\mu = 8.5132 \times 10^{-5}$, $m_1 = 1.4331$, $\beta = 0.466$, $\phi_d = 0.9975$, $F = 0.982$, $D_f = 1.346$, $N = 50$, and $\phi_c = 0.059$; for late-stage coarsening: $a_0 = 2.871$, $\mu = 0.99094$, $\Delta\mu = 9.1412 \times 10^{-5}$, $m_1 = 1.4339$, $\beta = 0.316$, $\phi_d = 1$, $F = 0.741$, $D_f = 1.817$, $N = 50$, and $\phi_c = 0.733$.

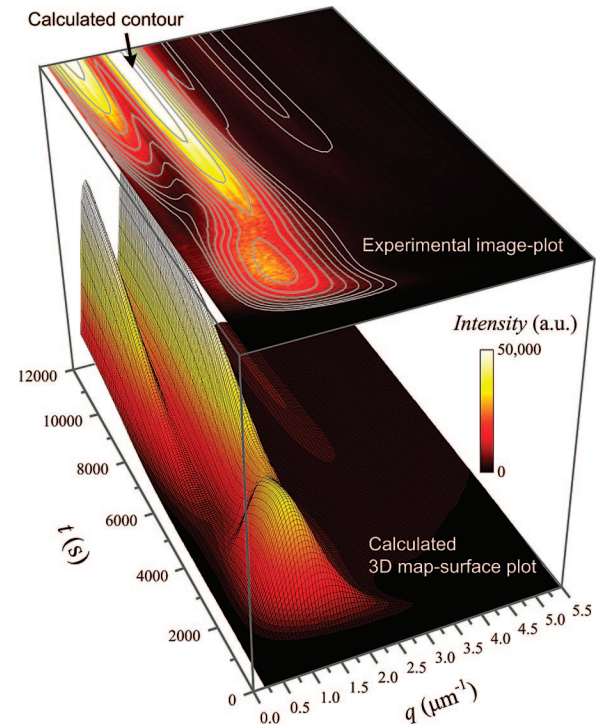

Figure 2. Comparison of the experimental H_v image plot ($\varphi = 45°$) for PVDF/TG-$LiCF_3SO_3$ solution ($\phi = 0.04$) at 293 K with the numerically calculated 3D map surface and contour plots.

and shined onto the sample. The sample cell was placed on THMS 600 heating and freezing stage (Linkam Scientific Co.), and the scattered light intensity was directly imaged through a Fourier lens and an analyzer onto the CCD camera (Apogee Instruments Inc., Alta U2000 CCD camera). The digitized images were transferred the real-time processing to a personal computer. In present study the reliable data are about scattering angle $\theta = 0.8°-22.5°$, corresponding to $q = 0.2-5.56\ \mu m^{-1}$ [$q = (4\pi m_1/\lambda)\sin(\theta/2)$, where q is the scattering vector, λ is the wavelength of incident light, and m_1 is the refractive index of an isotropic medium].

3.3. Scanning Electron Microscopy. The freeze-dried gel was prepared as follows: the 20 wt % homogeneous PVDF−DMSO/water (90/10) solution was quenched from 413 K to room temperature to form a wet gel and then placed into the freeze-drying equipment at 223 K. Under a vacuuming condition for more than 2 weeks, a dry gel was obtained. The morphology of the freeze-dried gel was investigated using scanning electron microscopy (SEM; Cambridge S-360).

4. Results and Discussion

Figure 1a shows the behavior of the H_v scattering profiles ($\varphi = 45°$) in different stages of gelation for PVDF/TG-$LiCF_3SO_3$ solution ($\phi = 0.04$) at 293 K. The solid lines show the best-fitted theoretical profiles by our model. A comparison of the experimental (left half of patterns) and the theoretical (right half of patterns) patterns is also shown in Figure 1b. It is clear that the theoretical patterns are in complete agreement with the experimental ones and hold the key feature of each evolution stage. The typical four-leaf-clover pattern characterizes the nucleation and growth stage, the four-crescent-moon pattern with a counterintuitive process (i.e., the reverse growth of q_m and a decrease in peak intensities) characterizes the aggregation/transition stage, and the emergence with steep growth of new first-order peak characterizes the late-stage evolution. In order to obtain more valuable information, these preliminary results should be further expanded and replicated.

A systematic stepwise survey of time-resolved scattering profiles was used to extract the essential parameters and to reconstruct the important events during the evolution. The reconstructed 3D map surface in Figure 2 reveals all the details of the gelation process. The complete agreement between the experimental image plot and the calculated contour plot indicates that the scattering modeling is practicable.

Thus, we can try to provide a much more detailed examination on the quantitative structure−evolution relationship. Figure 3 shows the behavior of the parameters a_0, a_r, β, ϕ_d, ϕ_c, μm_1, $\Delta\mu m_1$, and m_1 and represents the complete result to date in obtaining information on aspects of a complex event in gelation. In order to methodically depict what happens in that process, it would be useful to differentiate the evolution into three stages: (I) nucleation and growth, (II) aggregation, and (III) late-stage coarsening.

4.1. Nucleation and Growth Stage. Figure 3a shows two typical features of nucleation and growth behavior. First, m_1 increases gradually up to the value of the solvent—characterizing the growth of the PVDF microgels at the cost of the solute concentration in surrounding. Second, μm_1 is constant at this stage—characterizing the homogeneous composition of the growing microgels. On the other hand, $\Delta\mu m_1$ decreases continuously and approaches only slowly the end of this stage. We have known that $\Delta\mu m_1$ depends on the crystallinity and the orientation direction of crystalline grains within the microgels. Unlike typical model of polymeric spherulites, the decline of $\Delta\mu m_1$ means that the orientational correlation of the crystalline grains is a_0 dependent. This also clearly support the previous assumption which the PVDF microgel—as a spherical cluster

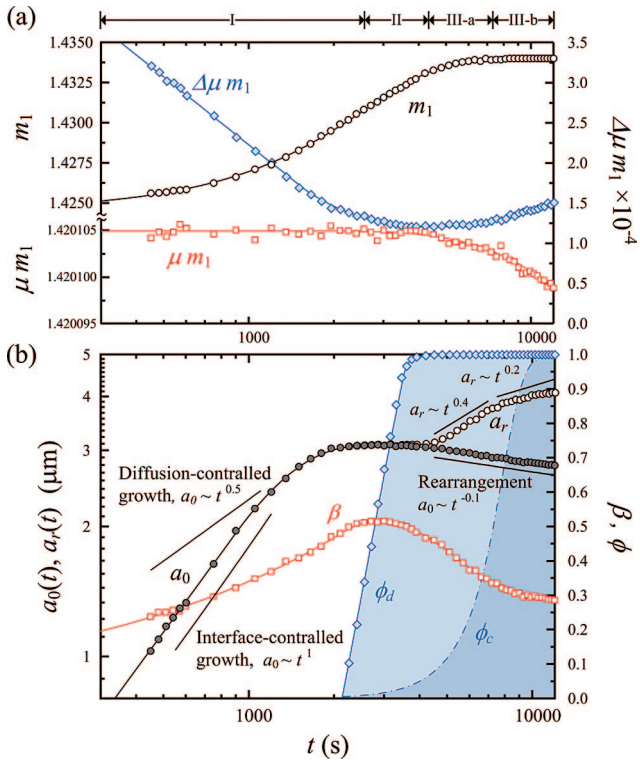

Figure 3. Parameters a_0, a_r, β, ϕ_d, μm_1, $\Delta\mu m_1$, and m_1 during the structural formation and evolution of nucleation gel: stage I, nucleation and growth; stage II, aggregation; stage III-a, diffusion-controlled coarsening; stage III-b, Ostwald ripening.

formed by the aggregation of crystalline microcolloids—belongs to the category 2 birefringent sphere.[7]

Instinctively, the nucleus of the microgel is surrounded by a concentration gradient which provides the driving force for microcolloid diffusion. It seems reasonable to deduce that the diffusion process may control the growth of the microgels; thus, the parabolic power law $a_0 \sim t^{0.5}$ should be expected. Surprisingly, as shown in Figure 3b, the growth exponent lies in between 0.9 and 1, indicating an interface-controlled growth. This linear growth causes us to associate similar behavior with the polymeric spherulites.[32] As distinct from the aggregation nature of the microgel, however, the formation and growth of polymeric spherulites is a typical solidification process, which depends on a competition between the impurity segregation (diffusion) and the liquid−solid interface propagation.[33−36] The interface-controlled growth behavior of the microgel may be explained by considering the competition between the nucleation density of the microgels and the diffusion distance of the crystalline microcolloids. If the diffusion distance is rather short, the interface reaction is likely to be the rate-controlling step. In this case, the higher solute (crystalline microcolloids) volume fraction and the exceptionally high nucleation density would be expected. With decreasing supersaturation (high temperature or low concentration), the long-range diffusion process would dominate the kinetic behavior.

As time goes on, the "solute" would be depleted gradually, and a_0 increases slowly and approaches the asymptotic regime. At the same time, $\Delta\mu m_1$ has reached its minimum value, predicting the end of growth behavior. On the other hand, as shown in Figure 3b, the gradual increase of β means the homogeneous nucleation process, which the nucleation is time dependent. At the end of the growth stage, β has reached its maximum value. In the subsequent stage, the aggregation and the coarsening processes would give rise to a change in β again.

4.2. Aggregation Stage. All the structural parameters of the primary microgel, with the exception of m_1, remain nearly constant in the this stage. However, we must mention here that the scattering pattern shows remarkable changes (i.e., the four-crescent-moon pattern and the counterintuitive growth process). The transition factor $F(q,\varphi)$, describing the local interference of the microgels, plays a large role in this stage.

The aggregation starts with the encounter of neighboring microgels and forms agglomerate or sphere doublet. Figure 3b shows that the volume fraction of the sphere doublet ϕ_d increases sharply from 0 to 1 and exhibits a critical-like behavior toward the end of the nucleation and growth stage (t > 2000 s). It is interesting to note that the experimental gel point and the time zone of $\phi_d = 1$ coincide on the time scale.[6] Often it is assumed that the gel must form by cluster−cluster aggregation process. Although the quantitative validity of the cluster volume fraction ϕ_c seems rather debatable, it may be deduced that the gelation would take place near $\phi_c = 1$. As the experimental gel point is much more close to $\phi_d = 1$, we may infer that neglecting the microgel volume fraction accounts for the observed discrepancy. If the microgel volume fraction is adequately high, the $\phi_d = 1$ may be associated with the jamming threshold. In our previous paper,[7] we have also shown that the PVDF gel is formed by a random packing of the microgels. These are why we said that the concept of the nucleation gel blurs the boundary between the gel and the jammed solid. In fact, the jamming is characterized by "dynamic arrest"; the present results, as probed by "static" light scattering, lack the ability to support these views. From a phenomenal point of view, ϕ_d, however, marks the starting point for the microgels aggregation. In the following, the m_1 reaches its asymptotic value 1.434, which suggests that the supersaturation is close to zero; the evolution has entered into late stage.

4.3. Late-Stage Coarsening. Generally, the size and internal structure of primary microgels should evolve during extended aging toward an asymptotic, time-invariant form, except for the occurrence of coarsening.[37] At first glance, surprisingly, the values of a_0, μm_1, and $\Delta\mu m_1$ still display a strong time dependence. For a_0 we find a law $a_0(t) \sim t^{-0.1}$, for μm_1 decreasing and close to the value of the PVDF is found, and for $\Delta\mu m_1$ we see a gradually increasing birefringence. All of these simply reflect the fact that the initial microgels collapse, leading to more compact and more anisotropic structures. On the other hand, as shown in Figure 3b, two distinct stages of the coarsening size a_r, each of which is well described by a power law, show a richness of the evolution phenomena.

4.3.1. Diffusion-Controlled Coarsening (Fast Process). In this stages, the coarsening is characterized by $a_r \sim t^{0.4}$, which indicates a diffusion process if the rearrangement of primary microgels ($a_0 \sim t^{-0.1}$) is considered. Additionally, β evolves and is subjected to a rapid drop with rather short aging periods. These mean that the gel network can immediately coarsen through further depleting the free small microgels from surroundings by diffusion. Because of the soft-colloid nature of the microgels, the hydrodynamic coalescence does not occur,[38−40] so that a rough surface with irregular warts is inevitable. Although, in general, the coarsening tends to favor homogeneous structures, or rather smooth or flat surface, in the present stage they are not directly related. This is easy to understand if we regard diffusion-controlled coarsening as a transition stage before the ripening is observed in the final stage.

4.3.2. Ostwald Ripening (Slow Process). The system tries to minimize its excess free energy by smoothing the rough surface. When the supersaturation is close to zero ($m_1 \rightarrow 1.434$) and the mesoscopic diffusion is restrained by the macroscopic gelation, the evaporation-condensation mechanism or Ostwald ripening is considered.[37] Figure 3b shows the experimental evidence for

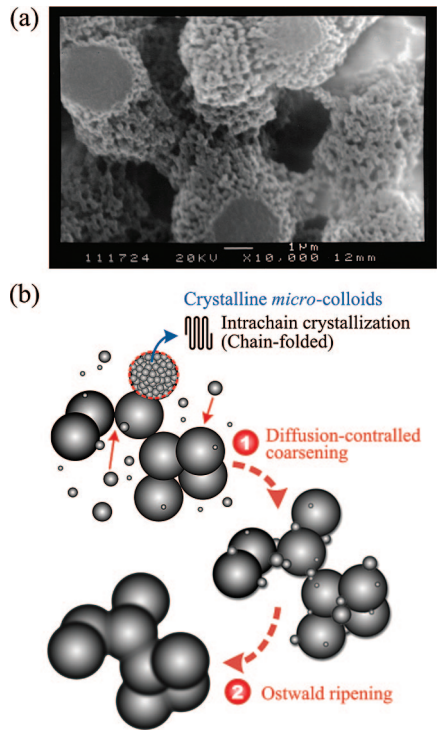

Figure 4. (a) SEM micrograph of a common representative of PVDF gel, prepared by the freeze-dried technique from 20 wt % PVDF−DMSO/water (90/10) gel. (b) Schematic representation of the structural formation and evolution of microgel in polymer solution. The model images that the microgels is constituted by a random assembly of crystalline microcolloids and highlights the "soft colloids" nature of PVDF microgels. The sketch also depicts what happens in the late-stage coarsening process of the nucleation gel.

the existence of this ripening process in the nucleation gel. In this stage, the behavior is characterized by $a_r \sim t^{0.2}$, which is closes to the predicted by the Lifshitz−Slyozov−Wagner theory (an exponent of 1/3) if $a_0 \sim t^{-0.1}$ is considered.[41,42] At the same time, β decreases slowly. From a phenomenological point of view, there is no reason to consider the dissolution of relatively stable crystal structure (i.e., crystalline microcolloid); thus, the ripening should take place via the crystalline microcolloids decomposition from small microgels and reprecipitation in the surface of backbone of the gel network or in the necks.

4.3.3. Compared with the Real-Space Structure. Figure 4a shows SEM micrograph of a common PVDF gel, prepared by the freeze-dried technique. The packing of spherical clusters is clearly discernible, and the size of the crystalline microcolloids is about 0.2 μm and is entirely consistent with Park and co-workers' result for the core−shell structure in dilute PVDF solutions ($R_b \sim 0.22$ μm, $R_H/R_g \sim 1.45$).[43] This micrograph visually proves the PVDF microgel is a nonequilibrium soft colloid, which the nonequilibrium means the aggregation and complex aging effect and the soft colloid means the relatively loose cluster and the rearrangeable structure. Figure 4b figuratively depicts what happens in the late-stage evolution process. It is interesting to note that besides reducing the surface free energy, the ripening also stiffens the weak network structure. The nucleation gels seem to show a richer structure and behavior than most idealized hard-sphere colloid systems.[44−46] Exploring the origin of the diverse gel morphologies has only been touched upon so far; however, the field will remain very active in the future.

5. Conclusion

In this paper, we have devised a scattering modeling that accurately reconstructs the entire course of physical gelation on the basis of elastic scattering theory. We have also shown how some essential parameters of gelation can be appropriately evaluated. Furthermore, on the grounds of our model, we can differentiate the gelation process into four stages in which the kinetic evolutions are predicted by either the growth or the coarsening theory.

An intuitive question goes as follows: whether nucleation−growth and aggregation are to be coincided on the time scale. Phenomenologically speaking, it could be possible. Nevertheless, the findings seemingly do not support this opinion. What factors have led to the two processes consecutive mechanism rather than concomitant one on the time scale? Probably the major reason is the fact that the nucleation−growth is a "local" enthalpy-driving process while the short-range attraction and the entropy play a dominant role in the origin of the "nonlocal" aggregation behavior,[47] and no evolutional competition−coupling relationships may exist between them.

In general, the nucleation and growth process trends to form a compact, spherical structure to minimize the surface energy; thus, the aggregation occurring, which results in an irregular, fingered cluster-structure, is unfavorable at this moment. Hence, in order to avoid aggregation, a "self-screening" effect may exist among the growing microgels. The self-screening may help account for why ϕ_d exhibits a critical-like behavior rather than exponential one. Close to the end of the growth stage, the system is regarded as colloidal dispersions, the self-screening effect must disappear, and the short-range attraction among the microgels and the entropy start dominating. Furthermore, for larger degree of supersaturation, where the system is far from equilibrium, we might speculate that the self-screening effect and critical-like behavior will smear out, and the concomitant process may occur. However, our discussions are still limited to a phenomenological level of description. To answer this question unequivocally, the time-resolved dynamic small-angle light scattering technique may be useful to examine whether certain "diffusive" relaxation modes exist during the nucleation and growth stage. Future research is obviously required, but now we leave this issue open.

On the other hand, let us devote a little more space to discussing β. The size distribution described for either stage is based on idealized assumption which is frequently not expected to be close to reality. The Gaussian distribution may only be fulfilled—if at all—during the earliest nucleation and growth stage; thus, β cannot quantitatively predict the feature of late-stage evolution. This may why the higher-order maximum or the shoulder, e.g., at $2.5 < q < 3.5$ μm^{-1} for $t = 8062$ s in Figure 1a, is still quantitatively off. From the Monte Carlo simulation, the theoretical results present a fairly clear picture on the "true" size distribution.[37] Introducing these more complex function into our model is not actually beneficial to describe late-stage evolution with quantitative accuracy. Indeed, up to now, analyzing the explicit form of the size distribution function on grounds of static scattering experiments is not feasible. From a practical point of view, the advantage of the scattering modeling is its simplicity and generality, while the excessive complication goes against our original intention and limits the practicality of the proposed methodology. However, this drawback does not limit or affect our interpretations.

In next work of this series, we will focus on the topic of global growth kinetics of the microgels. Although the scaling analysis of q_m and I_m is a fundamental issue, the relationship in H_v scattering is still unknown and uninvestigated. Having got the scaled form factor firmly established, we are now in a position to examine this topic. We will present a new relationship to describe the global growth kinetics of the microgels. Such research may have a contribution to make unraveling the

mystery of the nature of nonequilibrium soft colloids in nucleation gels.

Acknowledgment. The authors thank the National Science Council of the Taiwan for financially supporting this research under Contract NSC-95-2221-E-011-090-MY3.

References and Notes

(1) Guenet, J. M. *Thermoreversible Gelation of Polymers and Biopolymers*; Academic Press: New York, 1992.
(2) te Nijenhuis, K. *Adv. Polym. Sci.* **1997**, *130*, 1.
(3) Dikshit, A. K.; Nandi, A. K. *Macromolecules* **2000**, *33*, 2616.
(4) Dasgupta, D.; Manna, S.; Garai, A.; Dawn, A.; Rochas, C.; Guenet, J. M.; Nandi, A. K. *Macromolecules* **2008**, *41*, 779.
(5) Chou, C. M.; Hong, P. D. *Macromolecules* **2003**, *36*, 7331.
(6) Chou, C. M.; Hong, P. D. *Macromolecules* **2004**, *37*, 5596.
(7) Chou, C. M.; Hong, P. D. *Macromolecules* **2008**, in press.
(8) Cho, J. W.; Song, H. Y.; Kim, S. Y. *Polymer* **1993**, *34*, 1024.
(9) Vandeweerdt, P.; Berghmans, H.; Tervoort, Y. *Macromolecules* **1991**, *24*, 3547.
(10) Donald, A. M. *Soft Matter* **2008**, *4*, 1147.
(11) Stauffer, D.; Coniglio, A.; Adam, M. *Adv. Polym. Sci.* **1982**, *44*, 105.
(12) Coniglio, A.; Stanley, H. E.; Klein, W. *Phys. Rev. Lett.* **1979**, *42*, 518.
(13) Asnaghi, D.; Giglio, M.; Bossi, A.; Righetti, P. G. *J. Chem. Phys.* **1995**, *102*, 9736.
(14) Tromp, R. H.; Rennie, A. R.; Jones, R. A. L. *Macromolecules* **1995**, *28*, 4129.
(15) Takeshita, H.; Kanaya, T.; Nishida, K.; Kaji, K. *Macromolecules* **1999**, *32*, 7815.
(16) Hong, P. D.; Chou, C. M. *Macromolecules* **2000**, *33*, 9673.
(17) Lorén, N.; Altskär, A.; Hermansson, A. M. *Macromolecules* **2001**, *34*, 8117.
(18) Trappe, V.; Prasad, V.; Cipelletti, L.; Segre, P. N.; Weitz, D. A. *Nature (London)* **2001**, *411*, 772.
(19) Liu, A. J.; Nagel, S. R. *Nature (London)* **1998**, *396*, 21.
(20) Kanaya, T.; Takeshita, H.; Nishikoji, Y.; Ohkura, M.; Nishida, K.; Kaji, K. *Supramol. Sci.* **1998**, *5*, 215.
(21) Koizumi, S.; Annaka, M.; Borbely, S.; Schwahn, D. *Physica B* **2000**, *276*, 367.
(22) Koga, T.; Hashimoto, T.; Takenaka, M.; Aizawa, K.; Amino, N.; Nakamura, M.; Yamaguchi, D.; Koizumi, S. *Macromolecules* **2008**, *41*, 453.
(23) Stein, R. S.; Rhodes, M. B. *J. Appl. Phys.* **1960**, *31*, 1873.
(24) Meeten, G. H.; Navard, P. *J. Polym. Sci., Part B: Polym. Phys.* **1989**, *27*, 2023.
(25) Motegi, M.; Oda, T.; Moritani, M.; Kawai, H. *Polym. J.* **1970**, *1*, 209.
(26) Stanley, H. E.; Ostrowski, N. *On Growth and From: Fractal and Non-Fractal Patterns in Physics*; Nijhoff: Dordrecht, 1986.
(27) Dubois, J.; Fyen, W.; Rusu, D.; Peuvrel-Disdier, E.; Navard, P. *J. Polym. Sci., Part B: Polym. Phys.* **1998**, *36*, 2005.
(28) Roe, R. J. *Methods of X-ray and Neutron Scattering in Polymer Science*; Oxford University Press: New York, 2000.
(29) Ferri, F.; Greco, M.; Arcovito, G.; Bassi, F. A.; Spirito, M. D.; Paganini, E.; Rocco, M. *Phys. Rev. E* **2001**, *63*, 031401.
(30) Peuvrel, E.; Siegert, D.; Navard, P.; Meeten, G. H. *J. Polym. Sci., Part B: Polym. Phys.* **1992**, *30*, 865.
(31) Holoubek, J. *J. Polym. Sci., Part B: Polym. Phys.* **1994**, *32*, 351.
(32) Bassett, D. C. *Principles of Polymer Morphology*; Cambridge University Press: New York, 1981.
(33) Keith, H. D.; Padden, F. J. *J. Appl. Phys.* **1964**, *35*, 1270.
(34) Keith, H. D.; Padden, F. J. *J. Appl. Phys.* **1964**, *35*, 1286.
(35) Tanaka, H.; Nishi, T. *Phys. Rev. A* **1989**, *39*, 783.
(36) Gránásy, L.; Pusztai, T.; Tegze, G.; Warren, J. A.; Douglas, J. F. *Phys. Rev. E* **2005**, *72*, 011605.
(37) Wagner, R.; Kampmann, R.; Voorhees, P. W. In *Phase Transformations in Materials*; Kostorz, G., Ed.; Wiley-VCH: Weinheim, 2001; Chapter 5, pp 309−408.
(38) Nikolayve, V. S.; Beysens, D.; Guenoun, P. *Phys. Rev. Lett.* **1996**, *76*, 3144.
(39) Rosenfeld, G.; Morgenstern, K.; Esser, M.; Comsa, G. *Appl. Phys. A: Mater. Sci. Process.* **1999**, *69*, 489.
(40) Tanaka, H. *J. Chem. Phys.* **1996**, *105*, 10099.
(41) Lifshitz, I. M.; Slyozov, V. V. *J. Phys. Chem. Solids* **1961**, *19*, 35.
(42) Wagner, C. *Z. Electrochem.* **1961**, *65*, 581.
(43) Park, I. H.; Yoon, J. E.; Kim, Y. C.; Yun, L.; Lee, S. C. *Macromolecules* **2004**, *37*, 6170.
(44) Poon, W. C. K.; Haw, M. D. *Adv. Colloid Interface Sci.* **1997**, *73*, 71.
(45) Lattuada, M.; Wu, H.; Morbidelli, M. *Langmuir* **2004**, *20*, 4355.
(46) Taboada-Serrano, P.; Chin, C. J.; Yiacoumi, S.; Tsouris, C. *Curr. Opin. Colloid Interface Sci.* **2005**, *10*, 123.
(47) Kleman, M.; Lavrentovich, O. D. *Soft Matter Physics*; Springer: New York, 2003.

MA800788J